Fluid displacement patterns in porous media – 3D pore-network modeling

Schémas du déplacement des fluides en milieu poreux – Modélisation 3D de réseaux de pores

Nariman Mahabadi, Jaewon Jang
School of Sustainable Engineering and the Built Environment
Arizona State University, USA, jjang19@asu.edu

ABSTRACT: Multiphase fluid flow in porous media is found in various areas such as oil and gas recovery, hydrology, geological CO_2 sequestration, and soil remediation. The preferential flow channel formed by invading fluid is a critical constraint in those processes. In this study, a three-dimensional pore network model is employed to explore the pore scale characteristics affecting the displacement pattern. A wide range of capillary numbers and viscosity ratios is adopted in a time-dependent two-phase flow simulation. The results show that wider statistical pore size distribution and higher pore connectivity results in higher saturation of the invading fluid for all the three major flow regimes including viscous fingering, capillary fingering and stable displacement. The boundary between stable displacement and capillary fingering regime becomes indiscernible for the networks of uniform statistical pore size distribution and low pore coordination number. The boundary of viscous fingering regime moves to higher viscous numbers (higher logM) as the pore size variation decreases or pore connectivity increases.

RÉSUMÉ : Les fluides multiphasiques qui coulent dans des milieux poreux se trouvent dans diverses places telles que la récupération du pétrole et du gaz, l'hydrologie, la séquestration géologique du CO2 et l'assainissement des sols. Le canal d'écoulement préférentiel formé par le fluide envahissant est une contrainte critique dans ces processus. Dans cette étude, un modèle tridimensionnel du réseau poreux est utilisé pour explorer les caractéristiques de l'échelle des pores affectant le schéma du déplacement. Une large gamme de numéros capillaires et de rapports de viscosité est adoptée dans une simulation de flux biphasée et liée au temps. Les résultats montrent qu'une distribution statistique plus large de la taille des pores et une connectivité plus élevée des pores résulte dans une saturation plus élevée du fluide envahissant pour tous les trois principaux régimes d'écoulement, y compris la digitation visqueuse, la digitation capillaire et de déplacement stable. La limite entre le déplacement stable et le régime de la digitation capillaire devient indiscernable pour les réseaux de distribution statistique uniforme de la taille des pores et du nombre faible de coordination des pores. La limite du régime de digitation visqueuse se déplace vers des nombres visqueux plus élevés (logM plus élevé) à mesure que la variation de la taille des pores diminue ou la connectivité des pores augmente.

KEYWORDS: multiphase fluid flow, displacement pattern, pore-network modeling

1 INTRODUCTION

Multiphase fluid flow in porous media is found in various applications such as oil and gas recovery, hydrology, geological CO_2 sequestration, and soil remediation. The formation of preferential flow channels by invading fluid is a critical constraint in above processes. The two-phase displacement where a non-wetting fluid displaces a wetting fluid depends on several factors such as viscosity, interfacial tension, injection rate, wettability and characteristics of the porous media. A clear perspective of the structure and formation of the preferential pathways and its dependency on different parameters remains a challenge.

Lenormand et al. [1988] conducted a comprehensive study through pore network model simulations and micromodel experiments. They show three fluid displacement patterns: viscous fingering, capillary fingering and stable displacement regimes plotted on a logM–logC phase diagram. Here, M defines the viscosity ratio (ratio of the invading fluid viscosity μ_{inv} to the defending fluid viscosity μ_{def}) and *C* is the capillary number (the ratio of the viscos force to the capillary force).

$$M=\frac{\mu_{inv}}{\mu_{def}} \quad \text{Viscosity ratio} \quad (1)$$

$$C=\frac{q\mu}{A\gamma\ cos\theta} \quad \text{Capillary number} \quad (2)$$

Where q is the displacing fluid flow [m^3/s], A [m^2] is the cross sectional area of the inlet, and γ [N/m] is the interfacial tension between two fluids.

The physical interpretation of the three different regimes was explained as the following: (1) Viscos fingering: the principal force is due to the viscosity of the displaced fluid and capillary effect in the displacing fluid is negligible. The pattern includes spread tree-like fingers with no loops. In this case, the final saturation is low. (2) Capillary fingering: this occurs at low capillary numbers where viscous forces are negligible in both fluids and the principal force is due to capillarity. The pattern includes fingers growing in all directions with some loops that trap clusters of displaced fluid. The final saturation in this case is higher than the viscous fingering and lower than the stable displacement condition. (3) Stable displacement: this takes place at high capillary numbers and viscosity ratios where the principal force is due to the viscosity of the invaded fluid. The invading front is a flat front shape with a small number of irregularities and only a few trapped clusters of the displaced fluid. The final saturation is higher than viscous and capillary fingering, and close to a fully saturated condition.

A recent experimental study [*Zhang et al.*, 2011] confirmed the three displacement domains and their boundaries. They conducted a series of displacement experiments using a homogenous water-wet micromodel for different pairs of wetting- and non-wetting fluids with viscosity ratio M ranging from log =-1.95 to 1.88 and capillary number C ranging from logC=-5.88 to -1.02. Although their results confirmed the numerical results obtained by [*Lenormand et al.*, 1988], they modified the boundaries of displacement patterns. A more recent study [*Liu et al.*, 2013] used Lattice Boltzmann method to simulate immiscible fluid flow in a homogenous pore network model. Figure 1a illustrates the obtained displacement regimes and their boundaries proposed by *Lenormand et al.* [1988], *Zhang et al.* [2011] and *Liu et al.* [2013]. It was discussed that the discrepancy between the boundaries is due to the variation in the size and configuration (pore size distribution and manufacturing) of the pore networks.

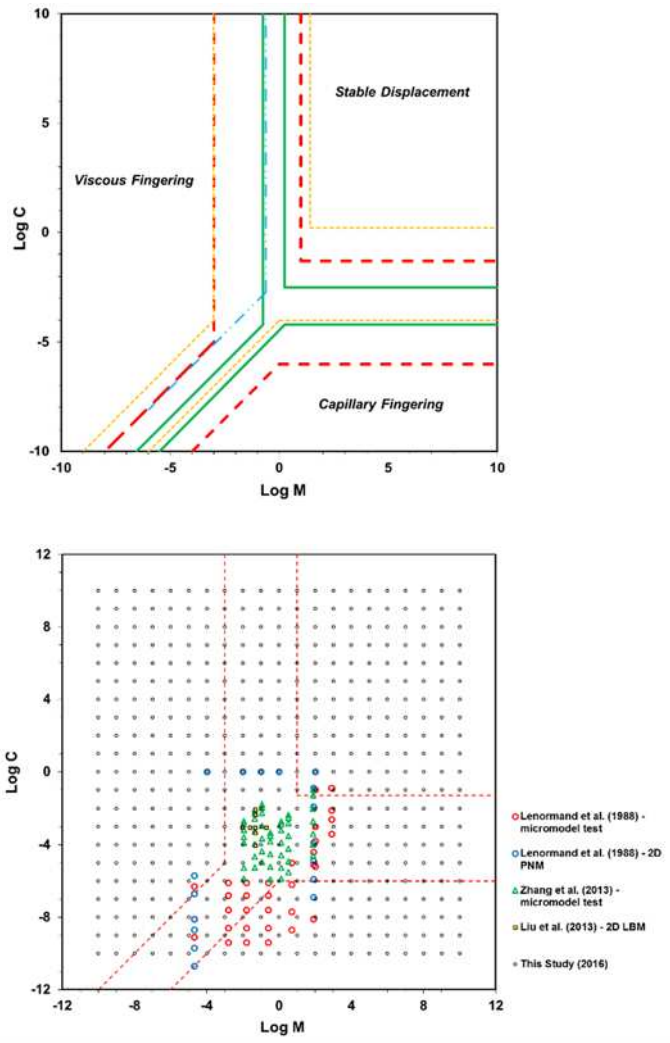

Figure 1. (a) Phase diagram boundaries suggested by Lenormand et al. [1988] (experimental study by red dashed and 2D pore network simulation by yellow small dashed-lines), Zhang et al. [2011] (experimental study by green solid line) and Liu et al. [2013] (2D Lattice Boltzmann simulation by blue dash dot-dotted lines). (b) Range of the selected pairs of Log C and Log M data used in Lenormand et al. [1988], Zhang et al. [2011], Liu et al. [2013] and the present study [2016] (The red dotted-lines shows the phase diagram proposed by Lenormand et al. [1988])

Figure 1b shows the range of capillary numbers and viscosity ratios used in above studies as well as this study. As shown in Figure 1b, the range of the data is limited compare to the proposed zones of the phase diagram because of difficulties in experiments (e.g., limited range of viscosity ratios for different fluid types) and numerical simulations (e.g., convergence problem in LBM especially for high and low viscosity ratio region).

This study employs a time-dependent two-phase flow simulation using a three-dimensional pore network model to explore the displacement patterns for a wide range of capillary numbers and viscosity ratios. The mechanisms of the three regimes are investigated particularly for a wide range of dimensionless numbers that were not covered in the previous studies. Moreover, all the recent numerical simulations use artificial two-dimensional pore network models that do not represent the heterogeneity of the real pore space. In order to deal with this problem, we use a 3D pore network model extracted from micro-CT images of sandy sediment to simulate the immiscible fluid flow through the porous medium. Moreover, the effect of statistical pore size distribution and pore connectivity on the preferential channel and fluid displacement patterns is explored.

2 NUMERICAL METHOD AND PROCEDURE

2.1 *3D Pore-network model*

A sediment recovered from Mallik 5L-38 site at 1,091meter depth is used for X-ray CT scanning and pore network extraction (for more information about the configuration and procedure used for X-ray CT scanning refer to *Mahabadi et al. [2016]*). In this study, the volume of the scanned image is 8mm^3 (2mm×2mm×2mm) with 12.5µm pixel resolution. A three-dimensional pore network consisting of spherical pores and cylindrical tubes is extracted from the CT images using the maximal ball algorithm developed by *Silin and Patzek* [2006]. The maximal ball algorithm searches for spheres inscribed in the pore wall. Then, the big spheres located in the center of pore spaces of the sediment grains become pores of the pore-network model and the small spheres inscribed in pore throats are turned into tubes. Further information on inscribing spheres and assigning spheres for pores or tubes is found in *Dong and Blunt* [2009]. The obtained pore network model consists 1425 pores and 5775 tubes with a mean tube connectivity per pore (coordination number cn) of cn=8.0. Mean pore radius is $\mu[R_{pore}]$=67µm, and mean tube size is $\mu[R_{tube}]$=12µm.

The 3D pore network model allows us to explore the effect of pore scale characterizations including the pore size distribution and connectivity.

The effect of pore size on the preferential flow regimes is explored using four different tube size distribution cases which include the original pore network model extracted from the CT images and the three other cases that are numerically generated by modifying only the tube size distribution of the network (size of balls, coordination number, location of pores and length of tubes are maintained constant). Figure 2 shows the four tube size distribution cases used in this study. The average value of tube size distribution is maintained constant while the standard deviation of tubes size distribution is varied from the original case (standard deviation σ) to higher (2σ) and lower (0.5σ and 0.1σ) cases.

The 2D network used in the literature has a constant coordination number cn=4. However, pore connectivity in real pore space (3D porous media) could have higher coordination numbers. The effect of connectivity is investigated using four different coordination numbers cn=8.0, 6.2, 5.1 and 4.6.

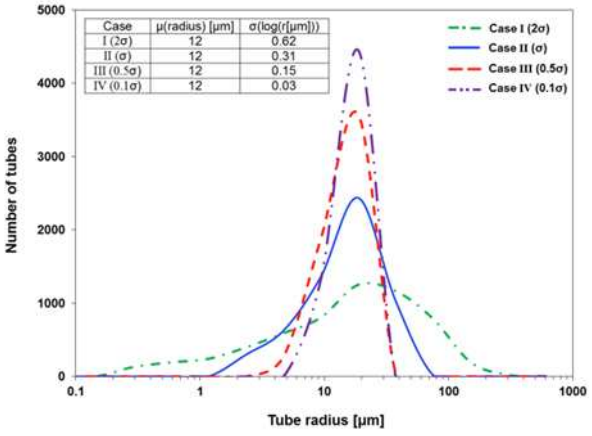

Figure 2. Different tube size distribution used in this study.

2.2 *Two-phase fluid flow simulation*

We follow the algorithm explained in *Aker et al.* [1988] to simulate two-phase immiscible fluid flow in the pore network model. Using this algorithm, we were able to model the dynamics of the temporal evolution of the fluid flow and the time dependency of the interface between the wetting and non-wetting fluids. To follow this algorithm, initially the pore network model is fully saturated by the defending fluid with viscosity μ_{def}, and the invading fluid with viscosity μ_{inv} is injected from the left boundary (inlet boundary) with a constant injection rate. All the boundaries are closed except the left (inlet) and right boundary (outlet). It is assumed that the fluids are immiscible so that there is an explicit interface between the defending and invading fluids

3 RESULTS N ANALYSIS

A total of 441 cases (21 viscosity ratios × 21 capillary numbers) are simulated for each of the tube size distribution and connectivity cn cases (totally 3528=441×4×4 simulations).

Figure 3 shows several simulations for different pairs of capillary number of viscosity ratio for tube size distribution case 2 (standard deviation =1σ). The simulation results clearly show the evolution of the phases from the viscous fingering to capillary fingering and stable displacement. At low viscosity ratio (LogM=-5) where the principal force comes from the viscosity of the displaced fluid, the displacement pattern has a tree-like shape and the final saturation of the invading fluid is very low. In this case (LogM=-5) the saturation slightly increases from 0.07 to 0.11 as the capillary number decreases (LogC decreases from 5 to -5). At low capillary number (Log C=-5) we observe that the displacement pattern changes from the viscous fingering to capillary fingering within the range of viscosity ratio from -5 to 5. The change of displacement pattern from capillary fingering to stable displacement is also shown in Figure 3, at which the viscosity ratio is high (LogM=5) and the capillary number increases from -5 to 5. The final saturation for the stable displacement condition is about 0.7 for this case.

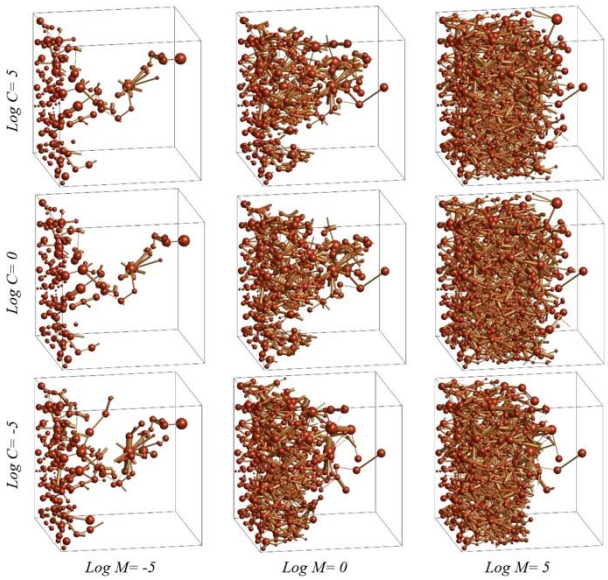

Figure 3. Selected simulations for different pairs of Log M and Log C numbers for tube size distribution case II (standard deviation = 1σ). The fluid flow direction is from the left to the right boundary.

The total length of the pore network model (2mm) is divided into five sections (the length of each section=0.4 mm) and the saturation of invading fluid is calculated for different pairs of logC and logM values in each section (Figure 4). The result clearly shows the evolution of flow patterns from viscous fingering (represented by blue points) to the capillary fingering and stable displacement zones (represented by red) points. The results for logM=5 and different logC=5, 0 and -5 show that the saturation of invading fluid increases with increasing capillary number especially at the intermediate zone of the network.

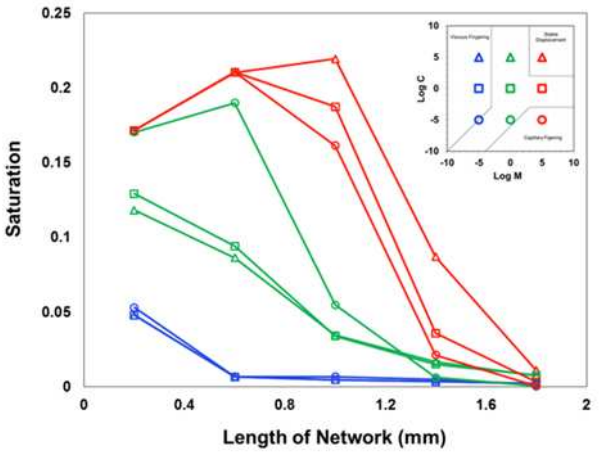

Figure 4. Saturation of invading fluid for different LogM and LogC numbers in different sections of the pore network model.

The results obtained from the large series of simulations are shown in terms of saturation using contour mapping for different statistical tube size distribution cases (Figure 5a) and different connectivity numbers cn (Figure 5b). Wider pore size distribution results in higher final saturation of invading fluid in all logC-logM regions. The stable displacement and capillary fingering zones merge together when the tube size distribution decreases significantly (similar to uniform pore size distribution). The same trend is also observed as the connectivity of pores decreases. The boundary of viscous fingering zone moves to higher logM (moves toward right size of phase diagram) as the distribution of pore size decreases.

4 CONCLUSIONS

The evolution of preferential patterns and phase diagram has been studied over the last decades. Recent numerical and experimental studies in the literature confirmed the three displacement domains (viscous fingering, capillary fingering and stable conditions). However, the boundaries of the proposed phase diagrams by different researchers vary. It was discussed that the discrepancy is due to the variation in the pore size and the configuration of the model. However, there is no comprehensive study available in the literature. Because of the difficulties involved in the numerical simulations and experimental methods, the previous studies only covers a limited range of fluids and injection rates.

In this study, a comprehensive study is conducted using a 3D pore network model to simulate the immiscible multiphase fluid flow for a wide range of capillary numbers and viscosity ratios. Four different tube size distribution and connectivity scenarios are simulated to explore the effect of pore scale characterizations on the saturation boundaries of phase diagram. Based on the results, higher pore size distribution and higher pore connectivity increase the saturation of invading fluid for all the three major flow regimes of viscous fingering, capillary fingering and stable displacement. The stable displacement and capillary fingering boundaries on the phase diagram merge together in uniform pore size distributions and low pore coordination numbers. The boundary of viscous fingering

regime moves to higher viscous numbers (higher log M) as the pore size variation decreases or pore connectivity increases.

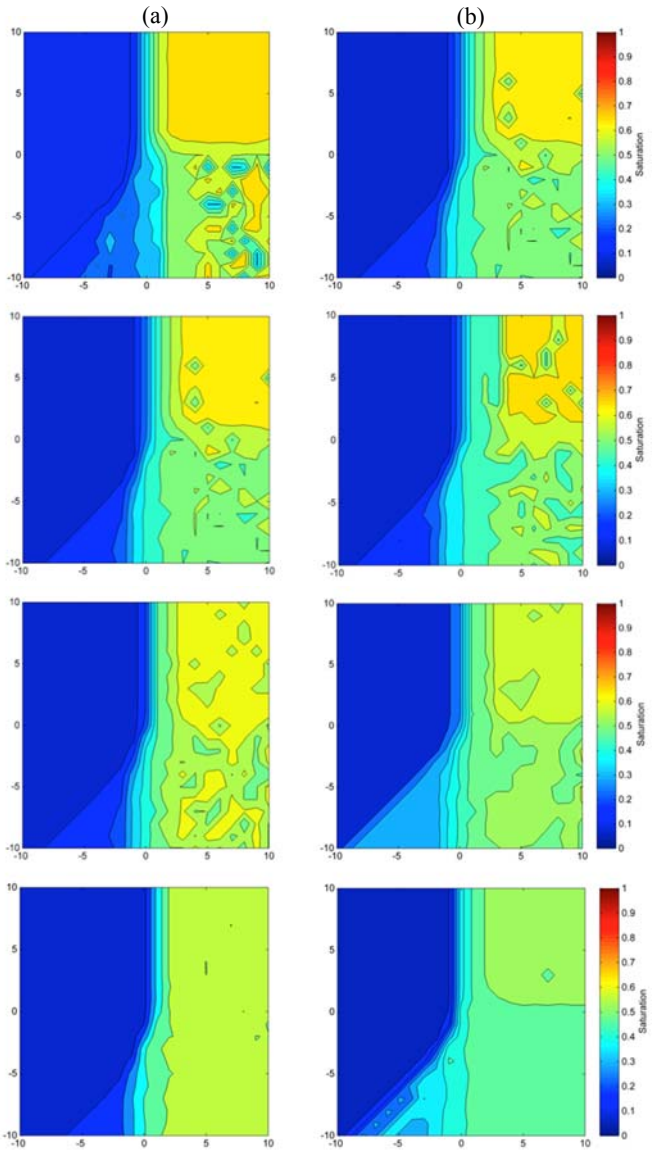

Figure 5. Saturation of invading fluid in Log M-Log C map. (a) Effect of different tube size distribtuions (2σ, σ and 0.5σ cases, from top to bottom). (b) Effect of connectivity for different coordination numbers cn=8.0, cn=6.2, cn=5.1 and cn=4.6 (from top to bottom).

5 ACKNOWLEDGEMENTS

The research is supported by the Dr. Jang's start-up fund provided by Arizona State University.

6 REFERENCES

Aker, E., K. Maloy, Jorgen, A. Hansen, and G. G. Batrouni (1988), A Two-Dimensional Network Simulator for Two-Phase Flow in Porous Media, Transport in Porous Media, 32, 163-186.

Dong, H., and M. Blunt (2009), Pore-network extraction from micro-computerized-tomography images, Physical Review E, 80(3), doi: 10.1103/PhysRevE.80.036307.

Lenormand, E. Touboul, and C. Zarcone (1988), Numerical models and experiments on immiscible displacements in porous media, J. Fluid Mech., 189, 165-187.

Liu, H., A. J. Valocchi, Q. Kang, and C. Werth (2013), Pore-Scale Simulations of Gas Displacing Liquid in a Homogeneous Pore Network Using the Lattice Boltzmann Method, Transport in Porous Media, 99(3), 555-580.

Mahabadi, N., Dai, S., Seol, Y., Yun, T. S., and Jang, J. (2016), The water retention curve and relative permeability for gas production from hydrate-bearing sediments: pore-network model simulation, Geochemistry, Geophysics, Geosystems, 17, 3099-3110.

Silin, D., and T. Patzek (2006), Pore space morphology analysis using maximal inscribed spheres, Physica A: Statistical Mechanics and its Applications, 371(2), 336-360.

Zhang, C., M. Oostrom, T. Wietsma, W, J. Grate, W, and M. Warner, G (2011), Influence of Viscous and Capillary Forces on Immiscible Fluid Displacement: Pore-Scale Experimental Study in a Water-Wet Micromodel Demonstrating Viscous and Capillary Fingering, energy&fules, 25(8), 3494-3505.